Article ID: 1006-8775(2018) 03-0323-11

# ASSESSMENT OF THE POEM2 MODEL FOR SIMULATING TROPICAL INTRASEASONAL OSCILLATION

WANG Kuo (王 阔)[1, 2, 3], MA Hao (马 浩)[1], LI Juan (李 娟)[3, 4], GU Bo-hui (顾伯辉)[2], WU Hao (吴 浩)[5]
(1. Zhejiang Climate Center, Hangzhou 310017 China; 2. College of Atmospheric Sciences, Lanzhou University, Lanzhou 730000 China; 3. International Pacific Research Center, University of Hawaii at Manoa, Honolulu 96822 USA; 4. Key Laboratory of Meteorological Disaster, Ministry of Education (KLME)/Joint International Research Laboratory of Climate and Environment Change (ILCEC)/Collaborative Innovation Center on Forecast and Evaluation of Meteorological Disasters (CIC-FEMD), Earth System Modeling Center, Nanjing University of Information Science and Technology, Nanjing 210044 China; 5. Hu'nan Climate Center, Changsha 410118 China)

**Abstract:** The intraseasonal oscillation (ISO) of the atmosphere is closely related to weather and climate systems and is also an important aspect of extended numerical weather forecast research. This phenomenon is significant in tropical regions and is one of the key indices for assessing the simulation capability of a climate model. To better evaluate numerical model simulations of the tropical ISO using the 10-year historic data calculated by the POEM2 climate system model developed by the University of Hawaii in the U.S., we utilized the methods of variance and power spectral analysis to compare and assess the simulation ability of this model for the ISO in tropical regions. Our results showed that the simulated variance results for the 850 hPa zonal wind and outgoing long-wave radiation (OLR) by POEM2 are overall consistent with the observed distribution pattern, and the simulated variance is relatively larger than the observed in the North Indian Ocean and West Pacific regions. With respect to the summer model, the winter model can better simulate the eastward propagation motion of the Madden-Julian oscillation (MJO) and the 850 hPa zonal wind. In comparison, the summer model can better simulate the northward propagation motion of MJO and atmospheric precipitation than the winter model. The eastward propagation speed of the simulated MJO signal is faster in the model than in the observation, and the high frequency region for the power spectra of meteorological element anomalies are concentrated in wavenumber 2 –3 in the simulation and in wavenumber 1 –2 in the observation. The multivariate combined empirical orthogonal function (EOF) results showed that this model can simulate the relationship between high-low level wind distributions and precipitation over the East Indian Ocean and the West Pacific, but the simulated signal is weaker than the observed. The lagging correlation of time coefficients between the first two EOFs from observation and simulation shows a similar cycle. Thus, these results indicate that in the future, the POEM2 climate system model needs to optimize the involved physical processes and parameterization scheme, strengthen the dynamic description of the mixed Rossby gravity wave, and improve the simulated ability of wavenumber 1.

**Key words:** model diagnostics; power spectrum analysis; POEM2 model; MJO
**CLC number:** P435 **Document code:** A
doi: 10.16555/j.1006-8775.2018.03.006

## 1 INTRODUCTION

Atmospheric intraseasonal oscillation (ISO) has been the focus of meteorologists since its discovery (Madden and Julian) [1, 2]. In addition to filling a gap between the weather and climate for the atmosphere, it can also provide a more scientific explanation for atmospheric interactions on multiple scales (Li [3]; Shi and Chen [4]; Lian et al. [5]). The formation and development of ISO are a result of non-linear interactions in the atmospheric interior, and they reflect the low-frequency remote response of atmosphere to the forcings of external boundary conditions (Li et al.[6]; Li and Xiao [7]). Regarding the temporal and spatial scales of atmospheric ISO, the kinetic propagation of ISO is a crucial atmospheric low-frequency signal on the extended scale, thus acting as one of the predictable sources for the 10 –30 day extended range weather forecast (Hendon et al.[8]; Wang et al.[9]). Therefore, ISO is closely related to studies on weather predictability (Ding et al. [10]; Zheng et al. [11]; Wang et al. [12]), interactions between atmospheric subcomponents on varying scales [13–15], and extended forecast improvement (Ding et al.[16]; Feng et al.[17]; Wang et al.[18]).

In tropical regions, the main ISO mode is the Madden-Julian oscillation (MJO), which is characterized by a distinct eastward propagation and strong convective activities [19]. A typical MJO event starts with the

**Received** 2017-09-14; **Revised** 2018-06-15; **Accepted** 2018-08-15
**Foundation item:** Natural Science Foundation of China (41605049, 41530531, 41475096); Key Special Scientific Research Fund of Meteorological Public Welfare Profession of China (GYHY201506001); Fund for Meteorological Science and Technology of Zhejiang Province, China (2017QN04)
**Biography:** WANG Kuo, Ph. D., senior engineer, primarily undertaking research on climate prediction and climate change.
**Corresponding author:** LI Juan, e-mail: juanl@nuist.edu.cn

convection-convergence ascending motion over the West Indian Ocean, which then horizontally moves eastward to the West Pacific along the zonal axis; during this period, convective precipitation concomitantly occurs, and the whole process lasts for approximately 40–50 days [20–21]. Regarding the dynamic mechanism, multi-scale (weather scale, intraseasonal scale, seasonal scale and even interannual scale) non-linear interaction is a basic factor in determining the formation and maintenance of MJO, while the temporal and spatial characteristics of MJO are influenced by the interactive effect of Rossby and wet Kelvin wave coupling [22–23]. Because the MJO populated region is located in the tropical Indian Ocean and Pacific, the formation and development of MJO are sensitive to the underlying ocean surface and are also closely related to tropical cyclones (TCs) and extreme precipitation[24–25]. In addition, the northward propagation wave induced by MJO significantly affects the precipitation in South Asia and East Asia monsoon regions, which are two of the most important monsoon regions around the globe, and in turn, this subject is an important component in the study of monsoon precipitation [26–27] and is closely related to the precipitation in China [28–29]. Consequently, assessment studies of relevant models have also been a focus. For instance, utilizing the 20th century simulated experimental result from the coupled model provided by IPCC AR4, Li and Yu [30] assessed model errors in simulating tropical cloud-climate feedback and compared the interannual feedback characteristics. In addition, on the basis of the simulated results of 24 IPCC AR4 models for the thermal controlling factors of TCs, Yu et al.[31] found that the sea surface temperature (SST) values simulated by most of the models are lower than the corresponding observations and that different models yielded increasing trends of varying magnitudes for the extended reconstructed SST (ERSST), which are distinctively different from the observations. Furthermore, Li et al. [32] introduced the analytic hierarchy process to assess the effect of TCs, and by adopting this method, the original observation data are directly calculated based on the corresponding weights and sorted from a comprehensive perspective, which avoids the problem of information overlap between different influencing factors.

Although the tropical ISO plays a key role in the weather and climate systems, strictly speaking, there is no single numerical model that can accurately reflect the observed main characteristics of the tropical ISO, mainly because of insufficient understanding of the latent heating process along the planet boundary layer[33], relatively low resolution in the General Circulation Model (GCM) model [34], and inaccurate cumulus parameterization scheme [35], according to previous studies. Moreover, the description of the MJO physical process requires further clarification, e.g., the dry Kelvin wave caused by non-linear heating and interactive coupling between wet Kelvin-Rossby waves, which causes difficulties for accurate model simulations [36–37]. To solve these problems, the International Pacific Research Center (IPRC) at the University of Hawaii in the U.S. developed a new climate model, the POP/CICE-OASIS-ECHAM model (POEM), which has been further developed and improved to POEM2 [38]. Xiang et al.[39] adopted this model for the SST forcing test and identified the main physical process of the feedback mechanism for the marine thermocline in the context of El Niño-Southern Oscillation. To assess the ability of the state-of-the-art numerical model in simulating the tropical ISO and to determine the possible cause of associated simulation errors, we will compare the simulated POEM2 model result on MJO with the corresponding observational result. The goal is to illustrate the pros and cons of this model for simulating the tropical ISO and to provide a reference for improving the ISO simulation ability of this climate model.

## 2 DATA AND METHODS

The outgoing long-wave radiation (OLR) data used in this study are the daily means of interpolated OLR data from 1979 to 2008 published by the National Oceanic and Atmospheric Administration (NOAA)[40]. The zonal wind data are the daily means of NCEP-DOE AMIP-II reanalysis zonal wind data published by the National Centers for Environmental Prediction/National Center for Atmospheric Research (NCEP/NCAR) [41], which have 17 vertical layers and a horizontal resolution of 2.5°× 2.5°. The precipitation data are the daily data published by the Global Precipitation Climatology Project (GPCP) [42].

The POEM2 model is an ocean-atmosphere coupled climate model developed by the International Pacific Research Center (IPRC) at the University of Hawaii. The updated POEM is further improved by coupling the POP ocean module developed by the U.S. Los Alamos National Laboratory [43] with the ECHAM atmosphere module developed by the Max Plank Meteorology Research Center in Germany [44], and with these updates, the POEM2 model becomes a climate system model including multi-sphere interactive processes between sea-land-ice-air and is capable of predicting climate for the atmosphere, land surface, ocean and sea ice on monthly, seasonal, and annual scales. The simulated data in this study are controlled experimental results: the aerosol and solar constants were fixed during the simulation process; the $CO_2$ level corresponds to the level in 1990; we chose 10-year data for comparison and analysis, and the observational data are from 1997 to 2006.

In this study, using the skill assessment criterion for weather forecast given by the World Meteorological Organization (WMO), we calculated the spatial anomaly

correlation of OLR (represented by the pattern correlation coefficient, PCC) to assess the forecast skill of the model. The equation is written as:

$$r=\frac{\sum_{i=1}^{n}(X_f-X_c-M_{f,c})_i(X_v-X_c-M_{v,c})_i\cos\varphi_i}{\sqrt{\sum_{i=1}^{n}(X_f-X_c-M_{f,c})_i^2\cos\varphi_i}\cdot\sqrt{\sum_{i=1}^{n}(X_v-X_c-M_{v,c})_i^2\cos\varphi_i}}$$

where $X_f$, $X_v$, and $X_c$ are the predicted value, observed value, and climate mean, respectively; $M_{f,c}$ and $M_{v,c}$ represent the deviation means of $X_f$ and $X_v$ from $X_c$, respectively; $n$ represents the number of grids in the chosen area; and $\cos\varphi_i$ is the latitude of grid $i$.

In addition, the methods adopted in this study include variance analysis, power spectral analysis and multi-variant EOF analysis for comparison and assessment of the observed and simulated data. To extract intraseasonal variables, some of the data in a period of 20–100 days were filtered via the Lanczos band pass.

## 3 RESULTS

### 3.1 *Total variance of the model*

The variance reflects the deviation degree of the data relative to the mean on average and is thus an important aspect for model assessment. In this study, we will first analyze the difference in the variance distribution between the observation and the simulation; then, we calculate the corresponding variances of intraseasonal subcomponents to study the percentages and contributions of the variances of intraseasonal variables to the original field. Fig.1 shows the observed and simulated variance distributions of the summer 850 hPa zonal wind. Compared to the corresponding variance in the observed original field, the simulated tropical summer 850 hPa zonal wind agrees with the observation that the wind field is higher in the south and north and lower in the center. Over the North Indian Ocean and the Bay of Bengal, the simulated variance values are slightly larger than the observations; after filtration, this phenomenon still exists, and the simulated 850 hPa zonal wind variance becomes stronger and more widely spread over the North Indian Ocean-West Pacific. A comparison of the variance values in the filtered field and the original field in Fig.1 (c and f) clearly illustrates that the simulated result is stronger in the North Indian Ocean compared to the observational result, which indicates a significant contribution from the variance of ISO in this region; in contrast, the simulated variance in the South Pacific is slightly weaker than the observed variance.

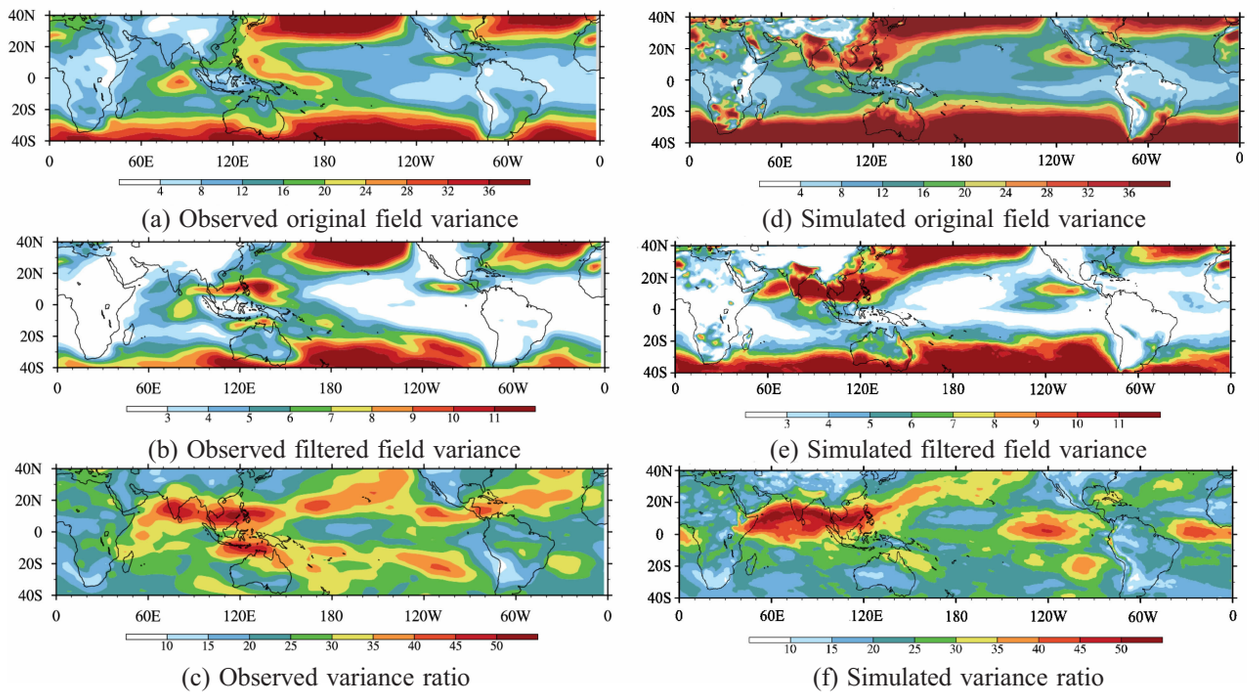


**Figure 1.** Observed summer 850 hPa zonal wind: (a) original field variance; (b) filtered field variance; (c) ratio of the variance of the filtered field to that of the original field. Simulated summer 850 hPa zonal wind (d, the same as (a)); (e, the same as (b)); (f, the same as (c)).

Figure 2 shows the observed and simulated variance distributions of summer OLR. Similar to Fig.1, the simulated variance is larger in magnitude and scale than the one from observation. For instance, in equatorial regions, the simulation is approximately 400–500 higher than the observed, especially in the tropical Atlantic Ocean where the simulation is twice the value from the observation. Additionally, the simulated

variance field after filtration is still stronger than that of the observation in magnitude and scale, and there is a high-value zone in the East Pacific that is almost negligible in the observed variance field and is thus worth attention. A comparison of the variance distributions between summer 850 hPa zonal wind and OLR in Figs.1 and 2 reveals that the magnitude and scale of the simulation are both larger than those of the observation, especially in regions from the North Indian Ocean and the Bay of Bengal to the West Pacific along the equator.

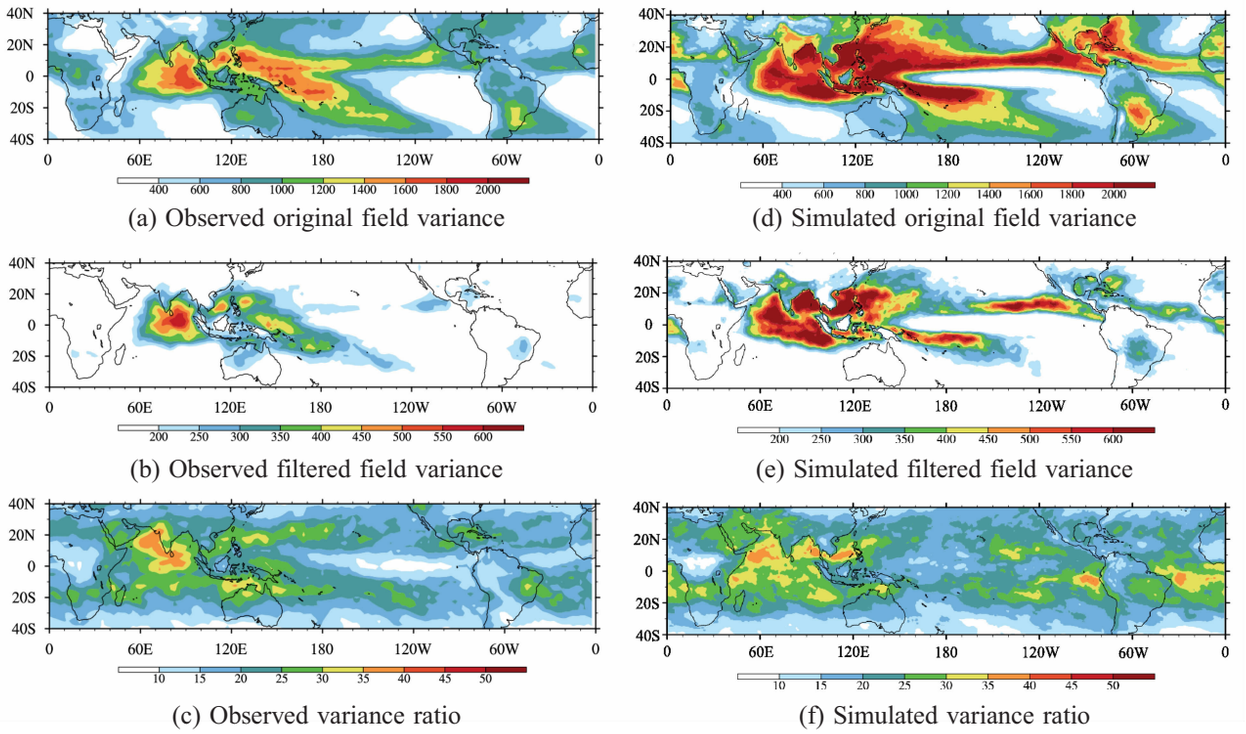


(a) Observed original field variance (d) Simulated original field variance

(b) Observed filtered field variance (e) Simulated filtered field variance

(c) Observed variance ratio (f) Simulated variance ratio

**Figure 2.** (a) to (f) are the same as (a) to (f) in Fig.1, but corresponding to OLR fields.

We also further compared the variance field distribution of the winter 850 hPa zonal wind (figures not shown) and found that the simulated result for the original field in marine regions between 20 –40° N is higher than the observed field. In addition, after filtration, the simulated 850 hPa zonal wind becomes stronger over the Central and East Indian Ocean and West Pacific along the equator. Conversely, the observed winter original field for the OLR variance shows a similar strength distribution compared to the corresponding summer field (figures not shown), but it is slightly larger over the East Indian Ocean and West Pacific along the equator. In comparison, the simulated result for the OLR variance is quite different in winter and summer, and the simulation amplifies the strength and scale mainly over the West Pacific at approximately 15°S in the Southern Hemisphere, which becomes more significant after filtration. The observed high values for the winter OLR variance ratio are mainly concentrated in the central-northern part of the Indian Ocean, while the simulated high values for the OLR variance ratio are distributed in most parts of the tropical Indian Ocean and a small part of the West Pacific. These facts illustrate that the model simulated variance is larger in strength and scale compared to the observed variance, which could result from the model's over-response to ocean-atmosphere coupling.

To directly assess the ability of the model in simulating meteorological elements on the tropical ISO scale, we filtered the precipitation field and 850 hPa wind field via the Lanczos band pass and compared their variance distribution patterns. Figs.3 and 4 mirror the observed and simulated variance fields for the filtered precipitation and 850 hPa zonal wind. A comparison of Fig.3a with Fig.4a reveals that the simulated precipitation distribution pattern is similar to the observed pattern, but the simulated strength is clearly higher than the observed on average. Specifically, the simulation value is approximately twice the observation value over the northern part of the Indian Ocean and the West Pacific, and the corresponding calculated PCC value is 0.69. The simulated winter 850 hPa zonal wind field is generally in agreement with the observation, but it is still relatively higher in high-value regions of the equatorial Indian Ocean and West Pacific; the corresponding calculated PCC value is 0.87. The summer model result is similar to the winter model result, but the PCC values for the summer precipitation and 850 hPa zonal wind are 0.76 and 0.85, respectively. Thus, based on our

comparison and assessment analysis on the tropical ISO scale and the calculated PCC values, we conclude that the POEM2 model better simulates precipitation in summer than in winter and better simulates the 850 hPa zonal field in winter than in summer. The tropical regions that have variance fields of varying strengths mainly include the Indian Ocean and the West Pacific, both of which are also key areas for the formation and development of MJO. In addition, Fig.4 shows that the simulated result is quite different from the observed result in this region. Thus, in the following sections, we will choose the tropical Indian Ocean as a key region to compare physical processes involved in the simulation with the corresponding observation.

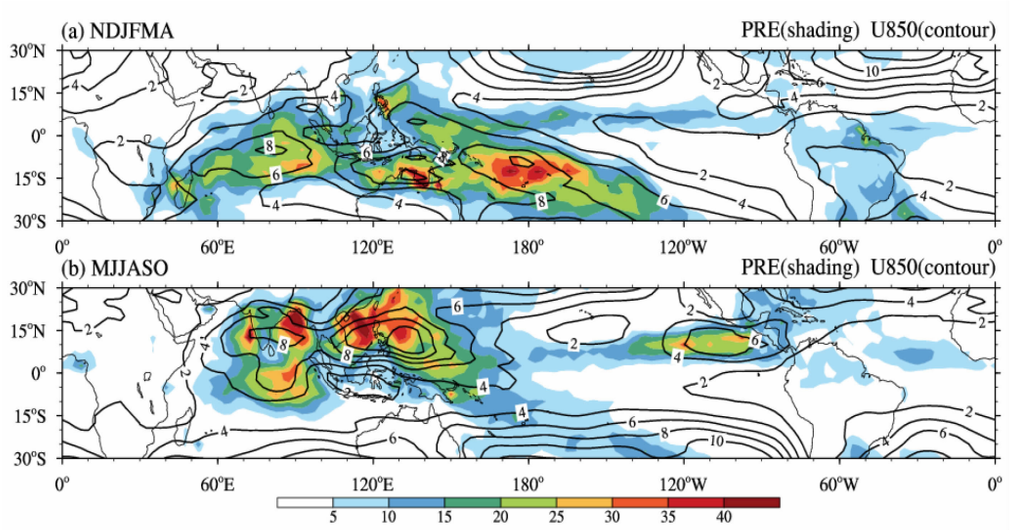


**Figure 3.** Observed variance fields of filtered precipitation and the 850 hPa zonal wind in (a) winter and (b) summer. The shade corresponds to precipitation, and the isolines represent 850 hPa zonal wind.

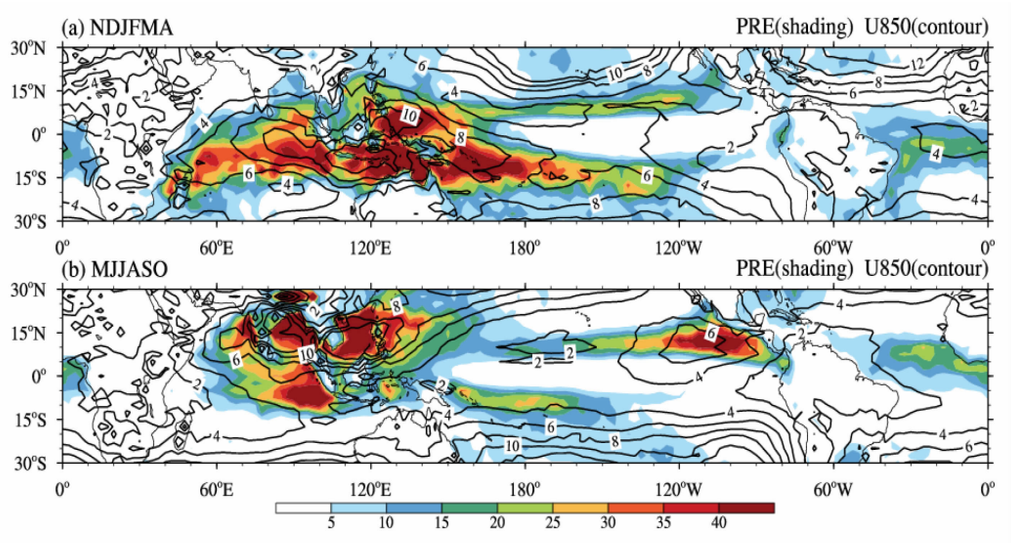


**Figure 4.** Same as Fig.3, but corresponding to the simulated result.

### 3.2 *Physical process in the key region*

To target the key region mentioned above, our discussion will focus on the Indian Ocean region (10°N–10°S, 80–100°E). Fig.5 shows the mean meridional and zonal distributions for the annual intraseasonal precipitation anomaly, 850 hPa zonal wind anomaly, and the lagging correlation of the intraseasonal precipitation. Fig.5a represents the observed distribution pattern of the mean meridional time lagging correlation between 10°N and 10°S. This figure clearly shows the MJO propagation characteristics at 30 –150° E, MJO propagates eastward with a significant phase speed, and the zonal wind anomaly appears approximately 5 –7 days later than the precipitation anomaly. The simulated result in Fig.5c also shows the eastward propagation characteristics, but the shades and isolines are "steeper" than those in the observation, implying that the simulated MJO propagates with a faster phase speed approximately 1.5–2 times the actual value.

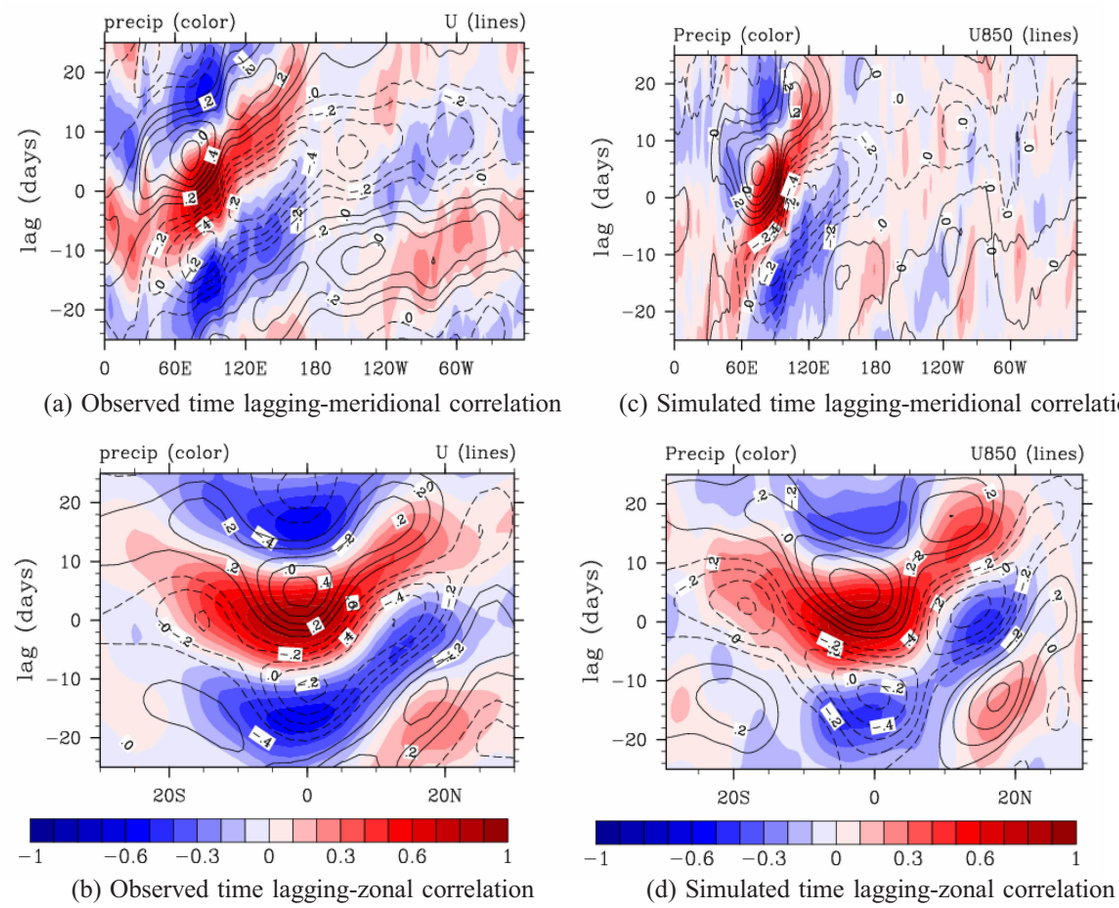


**Figure 5.** (a) Relationship between the observed annual mean time lagging-meridional intraseasonal precipitation anomaly and the 850 hPa zonal wind anomaly at 10° N–10° S with intraseasonal precipitation over the Indian Ocean; (b) same as (a), but corresponding to the observed mean time lagging-zonal correlation at 80° E–100° E; (c) same as (a), but corresponding to the simulated result; (d) same as (b), but corresponding to the simulated result. The shaded areas represent the correlation with the precipitation anomaly, and the isolines represent the correlation with the 850 hPa zonal wind anomaly.

In addition to propagating eastward, MJO also propagates northward. Thus, we adopted the same method and analyzed the northward propagation characteristics of MJO and the associated simulation ability of the model. Fig.5b shows the zonal correlation distribution of the observed mean time lagging at 80–100 °E. In this figure, MJO clearly propagates northward, and precipitation occurs approximately 5–7 days prior to the 850 hPa zonal wind. The simulated distribution pattern and phase speed in Fig.5 are similar to the observed pattern, which demonstrates the soundness of the model's simulation ability.

According to Fig.5, we found that the simulated annual MJO propagates eastward more quickly than the observation, while the simulated northward propagation agrees well with the observed. We also further simulated the MJO propagation characteristics in summer and winter using the POEM2 model, which were then compared with the observation (figures not shown). The results show that the simulated length of the eastward MJO propagation in summer related to the precipitation anomaly is shorter than the observed; the simulated result reflects the eastward propagation tendency of MJO in winter, but the simulated eastward propagation lasts longer than that of the observed and occurs at a higher speed. In contrast, the simulated MJO northward propagation in summer agrees well with the observed. Although the simulated result in winter also reflects the northward propagation of MJO, the simulated phase speed is slower than the observed, and the simulated 850 hPa zonal wind distribution does not correlate well with the observed. In general, the model can better simulate the eastward propagation of MJO in winter and the northward propagation of MJO in summer.

### 3.3 *Cause of model errors*

To analyze the internal characteristics of MJO in detail and determine the possible cause of model errors, we conducted a wavenumber frequency power spectral analysis of OLR and 850 hPa zonal wind anomalies to compare their differences in summer and winter. Fig.6 represents the wavenumber frequency power spectral analysis results for the OLR anomalies. This figure shows that the observed high-value regions on a 30–80

day scale in summer and winter are mainly composed of wavenumber 1 and wavenumber 1–2, respectively. In contrast, the simulated red high-value region is mainly composed of wavenumber 2 –3; additionally, the simulated temporal scale does not fall within the range of 30 –80 days, and the simulated frequency is lower than the observed.

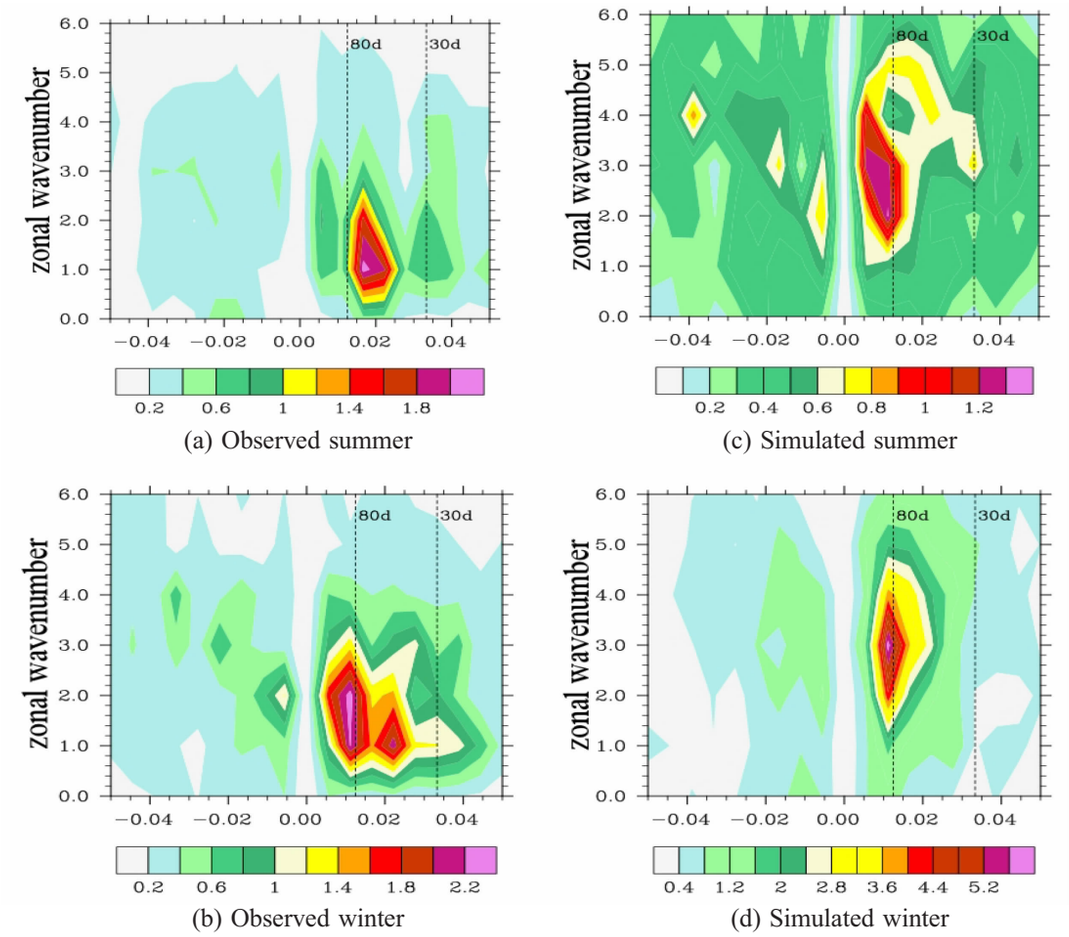


**Figure 6.** The mean OLR anomaly wavenumber-frequency diagrams at 10°N–10°S: (a) observed summer; (b) observed winter; (c) simulated summer; (d) simulated winter.

Similarly, we also conducted the wavenumber frequency power spectral analysis for the 850 hPa zonal wind anomalies in summer and winter as shown in Fig.7. On the scale of 30 –80 days, the observation is mainly composed of wavenumber 1, and the corresponding POEM2 simulation result in summer agrees well with the observation, thus generally representing the overall observed pattern. Conversely, the simulated winter 850 hPa zonal wind anomaly is mainly represented by wavenumber 2–3, while the observed is wavenumber 1–2. Thus, the mismatch between the simulation and the observation shows one of the main reasons for the model inaccuracy. In summary, the simulated result for the 850 hPa zonal wind anomaly by the POEM2 model is better than the simulated result for the OLR anomaly.

3.4 *Mutual configuration of model elements*

The multi-variable EOF analysis of OLR, the 850 hPa zonal wind and the 200 hPa zonal wind characterize the features of MJO [45] and verify whether these meteorological elements are mutually correlated. Fig.8 shows that over the East Indian Ocean and the West Pacific (70 –130° E), there are clear convective activities corresponding to the high and low air flow. In addition, the simulated result overall shows relatively weak oscillations in all the subcomponents, and the simulated variation trends of the 850 hPa and 200 hPa zonal winds are consistent with those from observations. However, the simulated OLR is different from the observed, which requires further improvement in the future. Inspection of the time lagging correlations of the EOF1 and EOF2 time coefficients shows that PC1 reaches the maximum correlation coefficient approximately 10 days ahead of PC2, while PC2 reaches the minimum correlation coefficient approximately 10 days ahead of PC1 with comparable magnitudes, indicating that the first two EOF modes are mutually inseparable. The POEM2 model also shows similar periodic variations, and the simulated wave peaks and wavelengths generally agree with the observation.

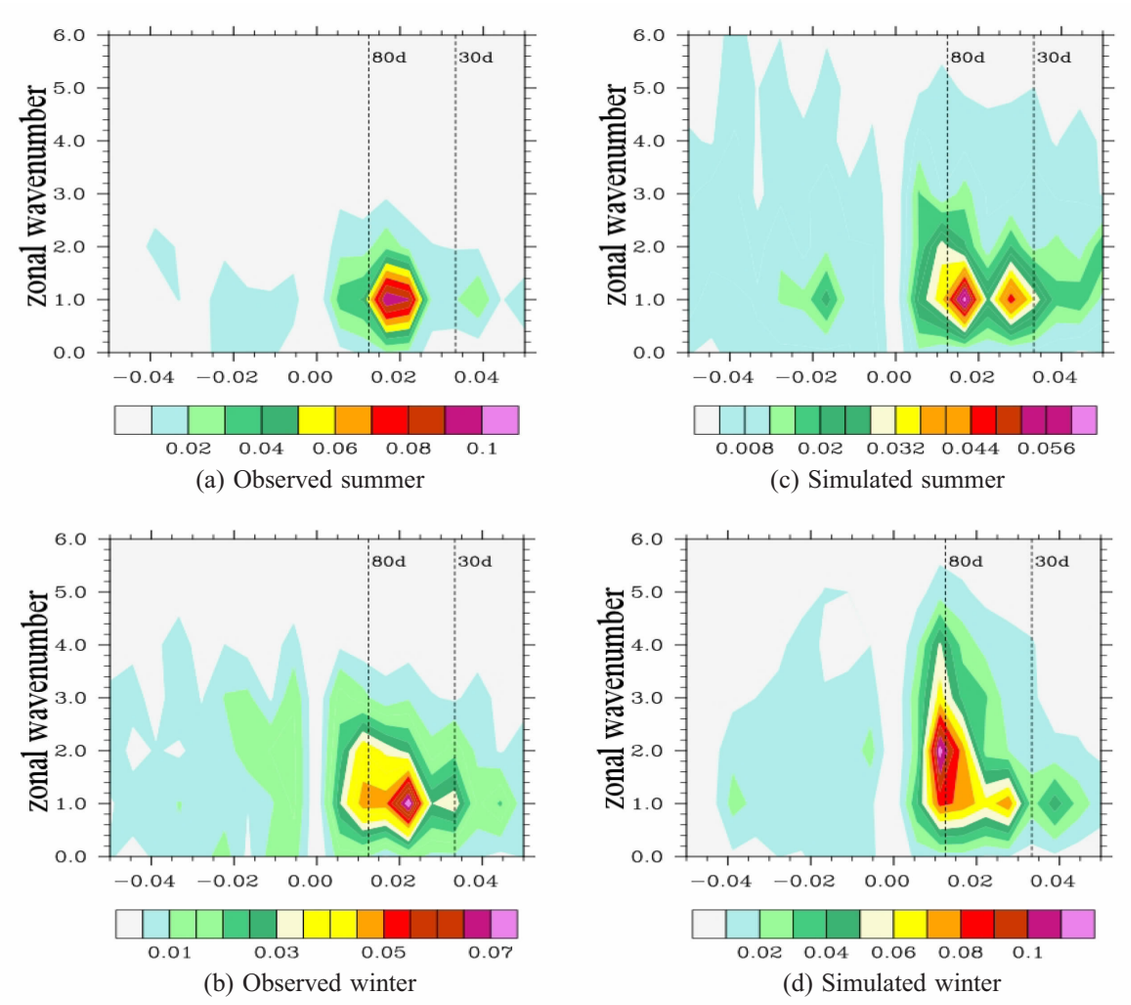


**Figure 7.** Same as Fig.6, but corresponding to the 850 hPa zonal wind anomaly (color bar unit: $m^2/s^2$).

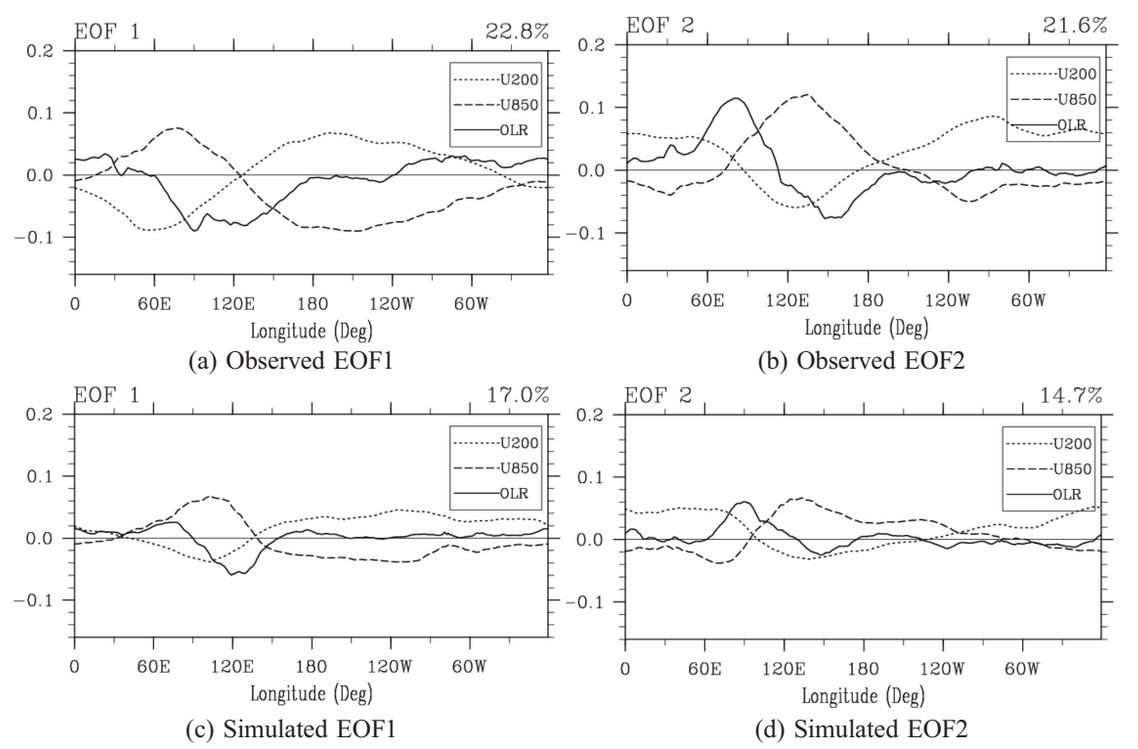

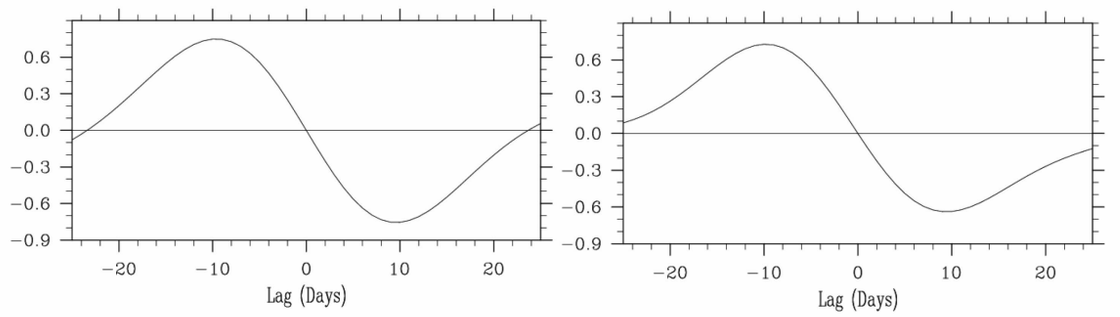


**Figure 8.** The mean multi-variable combined EOF at 15°N–15°S in all seasons: (a) observed EOF1; (b) observed EOF2; (c) simulated EOF1; (d) simulated EOF2, and the time lagging correlations between EOF1 and EOF2 time coefficients; (e) observation; and (f) simulation. The short dashed line represents 200 hPa zonal wind, the long dashed line 850 hPa zonal wind, and the solid line OLR. All the data were processed via filtration.

## 4 RESULTS AND DISCUSSION

In this study, by using the methods of variance analysis, band pass filtration, power spectral analysis, and multi-variable EOF, we assessed the ability of the POEM2 model to simulate the tropical ISO and found that this model can handle the overall distribution patterns of the 850 hPa zonal wind and OLR, but the simulated variance is larger than the observed in some regions, which might be related to over-coupling in the numerical model. The comparison and assessment analysis on different tropical intraseasonal scales showed that the model is relatively better at simulating the precipitation in summer and the 850 hPa zonal wind in winter compared to the observation results. We further targeted the Indian Ocean to analyze the physical processes that result in model deviations and found that the simulated eastward propagation speed of the MJO signal is approximately 1.5–2 times higher than the observed, implying that one possible reason for the overall simulation deviation is an inaccurate estimate of the MJO propagation. Relatively speaking, the model can better simulate the eastward propagation of MJO and the corresponding 850 hPa zonal wind in winter is better than that in summer. Conversely, the simulated northward MJO propagation and the corresponding precipitation in summer are better than those in winter.

The wavenumber frequency power spectra of OLR and the 850 hPa zonal wind illustrate that the simulated high-value region of the power spectra is concentrated at wavenumber 2–3 while the observed power spectra correspond to wavenumber 1–2, which demonstrates that the main frequency of the simulated result is higher than that of the observed result. Thus, this verifies that the simulated speed of the eastward MJO propagation is faster than the observed result. The multi-variable combined EOF result further illustrates that the model can best simulate the relationship between the high-low level wind and precipitation over the East Indian Ocean and the West Pacific. Although the variation trends of the simulated 850 hPa and 200 hPa zonal winds agree with the observed results, the simulation of OLR requires further improvement. The time lagging correlations of the time coefficients between the first two EOF modes in the POEM2 model also show similar periodic variations compared with the observation, and the simulated wave peaks and wavelengths generally agree with the observation results.

The University of Hawaii coupled the advanced atmosphere and ocean subcomponent models for the development of the POEM2 model. The results from this study show that the simulated variances of the tropical meteorological elements using this model are generally larger than the observed, and the simulated eastward propagation travels faster. To objectively match the observational data, we need to further optimize the involved dynamic physical processes and the parameterization scheme, strengthen the description of the mixed Rossby gravity wave, and further improve the ability of the numerical model in simulating wavenumber 1. Through the assessment of POEM2 model in this study, the knowledge of simulating ISO in tropical regions is deepened. However, it requires further work to reduce the main simulation errors in model in the future.

**REFERENCES:**

[1] MADDEN R A, JULIAN P R. Detection of a 40-50 day oscillation in the zonal wind in the tropical Pacific [J]. J Atmos Sci, 1971, 28(5): 702-708.
[2] MADDEN R A, JULIAN P R. Description of global-scale circulation cells in the tropics with a 40-50 day period [J]. J Atmos Sci, 1972, 29(6): 3138-3158.
[3] LI Chong-yin. The intraseasonal oscillation in atmosphere [J]. Chin J Atmos Sci, 1990, 14(1): 32-45.
[4] SHI Neng, CHEN Hui. The ultralong wave characteristics of the monthly mean height for the year of strong and weak Southern Oscillation (SO) at 500 hPa [J]. Sci Meteor Sinica, 1989, 9(2): 139-147.
[5] LIAN Yi, BUEH Cholaw, XIE Zuo-wei, et al. The

anomalous cold vortex activity in northeast China during the early summer and the low-frequency variability of the northern hemispheric atmosphere circulation [J]. Chin J Atmos Sci, 2010 34(2): 429-439.
[6] LI Chong-yin, CAO Wen-zhong, LI Gui-long. The effect of basic air flow on the instability of intraseasonal oscillation in the middle and high latitudes [J]. Sci China (Ser B), 1995, 25(9): 978-985.
[7] LI Chong-yin, XIAO Zi-niu. The warming of the equatorial eastern Pacific excited the 30-60 day oscillation of the global atmosphere [J]. Chin Sci Bull, 1991, 36 (15): 1157-1160.
[8] HENDON H H, LIEBMANN B, NEWMAN M, et al. Medium-range forecast errors associated with active episodes of the Madden-Julian oscillation [J]. Mon Wea Rev, 2000, 128(1): 69-86.
[9] WANG Kuo, FENG Guo-lin, SUN Shu-peng, et al. Study of the stable components in extended-range forecasting for the coming 10-30 days during the snow storm event in January 2008 [J]. Acta Phys Sinica, 2012, 61(10): 109201.
[10] DING Rui-qiang, LI Jian-ping, SEO K H. Estimate of the predictability of boreal summer and winter intraseasonal oscillations from observations [J]. Mon Wea Rev, 2011, 139(8): 2421-2438.
[11] ZHENG Zhi-hai, HUANG Jian-ping, FENG Guo-lin, et al. Forecast scheme and strategy for extended-range predictable components [J]. Sci China (Ser D), 2013, 56 (5): 878-889.
[12] WANG Kuo, FENG Guo-lin, ZENG Yu-xing, et al. Analysis of stable components in extended-range forecast for the coming 10-30 days in winter 2010 and 2011 [J]. Chin Phys B, 2013, 22(12): 570-577.
[13] SHI Neng, CAO Hong-xing. The temporal-spatial teleconnection structure of the precipitation field in China [J]. Sci Meteor Sinica, 1993, 13(3): 252-260.
[14] ZHAO Jun-hu, FENG Guo-lin, ZHI Rong. Progresses and prospects in research on season division and seasonal changes in China [J]. J Trop Meteor, 2013, 19(1): 28-38.
[15] LIU Fei, WANG Bin. A frictional skeleton model for the Madden-Julian oscillation [J]. J Atmos Sci, 2012, 69(9): 2749-2758.
[16] DING Rui-qiang, LI Jian-ping, SEO K H. Predictability of the Madden-Julian oscillation estimated using observational data [J]. Mon Wea Rev, 2010, 138 (3): 1004-1013.
[17] FENG Guo-lin, SUN Shu-peng, ZHAO Jun-hu, et al. Analysis of stable components for extended-range (10-30 days) weather forecast: A case study of continuous overcast-rainy process in early 2009 over the mid-lower reaches of the Yangtze River[J]. Sci China (Ser D), 2013, 56(9): 1576-1587.
[18] WANG Kuo, FENG Guo-lin, ZENG Yu-xing, et al. Extraction of 10-30-day stable components from a boreal atmosphere during ENSO phases[J]. Discrete Dyn Nature Soc, 2015, 2015(4): 1-6.
[19] WANG Bin, XIE Xiao-su. A model for the boreal summer intraseasonal oscillation [J]. J Atmos Sci, 1997, 54(1): 72-86.
[20] MALONEY E D, HARTMANN D L. Frictional moisture convergence in a composite life cycle of the Madden-Julian oscillation [J]. J Climate, 1998, 11 (9): 2387-2403.
[21] MALONEY E D. An intraseasonal oscillation composite life cycle in the NCAR CCM3.6 with modified convection [J]. J Climate, 2002, 15(9): 964-982.
[22] WANG Bin, RUI Hua-lan. Dynamics of the coupled moist Kelvin-Rossby waves on an equatorial beta-plane [J]. J Atmos Sci, 1990, 47(4): 397-413.
[23] LIU Fei, WANG Bin. Impacts of upscale heat and momentum transfer by moist Kelvin waves on the Madden-Julian Oscillation: A theoretical model study [J]. Clim Dyn, 2013, 40(1-2): 213-224.
[24] WANG Bin, XIE Xiao-su. Coupled modes of the warm pool climate system part I: The role of air-sea interaction in maintaining Madden-Julian Oscillation [J]. J Climate, 1998, 11(8): 2116-2135.
[25] JONES C. Occurrence of extreme precipitation events in California and relationships with the Madden-Julian oscillation [J]. J Climate, 2000, 13(20): 3576-3587.
[26] YASUNARI T. Cloudiness fluctuation associated with the Northern Hemisphere summer monsoon [J]. J Meteor Soc Japan, 1979, 57(3): 227-242.
[27] WANG Bin, WEBSTER P J, TENG Hai-yan. Antecedents and self-induction of the active-break Indian summer monsoon [J]. Goephys Res Lett, 2005, 32(4): L04704.
[28] FENG Guo-lin, ZHAO Jun-hu, ZHI Rong, et al. Recent progress on the objective and quantifiable forecast of summer precipitation based on dynamical-statistical method [J]. J Appl Meteor Sci, 2013, 24(6): 656-665.
[29] GU De-jun, JI Zhong-ping, LIN Ai-lan, et al. The oscillation of Guangzhou daily precipitation and its simple harmonic wave model for extended-range forecasts [J]. J Trop Meteor, 2013, 29(6): 899-906.
[30] LI Zhi-qiang, YU Yong-qiang. Assessment of cloud-climate feedback simulation bias of coupled ocean-atmosphere model in the tropical Pacific [J]. Chin J Atmos Sci, 2011, 35(3): 457-472.
[31] YU Jin-hua, TANG Sheng, WU Li-guang, et al. Assessments on simulation of thermodynamic parameters of tropical cyclone in IPCC-AR4 Models [J]. Acta Oceanol Sinica, 2011, 33(6): 39-54.
[32] LI Chun-mei, LUO Xiao-ling, LIU Jin-luan, et al. Application of analytical hierarchy process in the assessment model on tropical cyclone disaster's influence [J]. J Trop Meteor, 2006, 22(3): 223-228.
[33] LING Jian, LI Chong-yin, ZHOU Wen, et al. Effect of boundary layer latent heating on MJO simulations [J]. Adv Atmos Sci, 2013, 30(1): 101-115.
[34] JIA Xiao-long, LI Chong-yin, LING Jian, et al. Impacts of a GCM's resolution on MJO simulation [J]. Adv Atmos Sci, 2008, 25(1): 139-156.
[35] ZHANG G J, MCFARLANE N A. Sensitivity of climate simulation to the parameterization of cumulus convection in the Canadian Climate Centre General Circulation Model [J]. Atmos Ocean, 1995, 33: 407-446.
[36] WALISER D, SPERBER K, HENDON H, et al. MJO simulation diagnostics [J]. J Climate, 2009, 22 (11): 3006-3030.
[37] LI T. Recent advance in understanding the dynamics of the Madden-Julian oscillation [J]. J Meteor Res, 2014, 28 (1): 1-33.
[38] XIANG Bao-qiang, WANG Bin, LI T. A new paradigm for the predominance of standing Central Pacific Warming after the late 1990s [J]. Clim Dyn, 2013, 41(2):

327-340.
[39] XIANG Bao-qiang, WANG Bin, DING Qing-hua, et al. Reduction of the thermocline feedback associated with mean SST bias in ENSO simulation [J]. Clim Dyn, 2012, 39(6): 1413-1430.
[40] LIEBMANN B, SMITH C A. Description of a complete (interpolated) outgoing longwave radiation dataset [J]. Bull Amer Meteor Soc, 1996, 77: 1275-1277.
[41] KANAMITSU M, EBISUZAKI W, WOOLLEN J, et al. NCEP-DOE AMIP-II reanalysis (R-2) [J]. Bull Amer Meteor Soc, 2002, 83(11): 1631-1643.
[42] ADLER R F, HUFFMAN G J, CHANG A, et al. The version 2 global precipitation climatology project (GPCP) monthly precipitation analysis (1979-present) [J]. J Hydrometeor, 2003, 4(6): 1147-1167.
[43] SMITH R D, DUKOWICZ J K, MALONE R C. Parallel ocean general circulation modeling [J]. Phys D, 1992, 60 (1-4): 38-61.
[44] ROECKNER E, ARPE K, BENGTSSON L, et al. The Atmospheric General Circulation Model ECHAM-4: Model Description and Simulation of Present-day Climate [M]. Hamburg: Max-Planck-Institute for Meteorology Rep, 1996: 90-90.
[45] WHEELER M C, HENDON H H. An all-season real-time multivariate MJO index: Development of an index for monitoring and prediction [J]. Mon Wea Rev, 2004, 132 (8): 1917-1932.

**Citation:** WANG Kuo, MA Hao, LI Juan, et al. Assessment of the POEM2 model for simulating tropical intraseasonal oscillation [J]. J Trop Meteor, 2018, 24(3): 323-333.